Measuring time with different neural chronometers during a synchronization-continuation task

Hugo Merchant[1,2], Wilbert Zarco[1], Oswaldo Pérez, Luis Prado, and Ramón Bartolo

Department of Cognitive Neurocience, Instituto de Neurobiología, Universidad Nacional Autonoma de México, Campus Juriquilla, Queretaro 76230, Mexico

Edited by Ranulfo Romo, Universidad Nacional Autonoma de México, Mexico City, Mexico, and approved October 25, 2011 (received for review August 8, 2011)

Temporal information processing is critical for many complex behaviors including speech and music cognition, yet its neural substrate remains elusive. We examined the neurophysiological properties of medial premotor cortex (MPC) of two Rhesus monkeys during the execution of a synchronization-continuation tapping task that includes the basic sensorimotor components of a variety of rhythmic behaviors. We show that time-keeping in the MPC is governed by separate cell populations. One group encoded the time remaining for an action, showing activity whose duration changed as a function of interval duration, reaching a peak at similar magnitudes and times with respect to the movement. The other cell group showed a response that increased in duration or magnitude as a function of the elapsed time from the last movement. Hence, the sensorimotor loops engaged during the task may depend on the cyclic interplay between different neuronal chronometers that quantify the time passed and the remaining time for an action.

medial premotor area | timing neurophysiology | supplementary motor area

Interval timing in the milliseconds is a prerequisite for many complex behaviors, such as the perception and production of speech (1), the execution and appreciation of music and dance (2, 3), and the performance of a large variety of sports (4). Time in music comes in a variety of patterns, which include isochronous sequences where temporal intervals are of a single constant duration or, more commonly, sequences containing intervals of many durations. In addition, the ability to capture and interpret the beats in a rhythmic pattern allows people to move and dance in time to music (3). Music and dance, then, are behaviors that depend on intricate loops of perception and action, where temporal processing can be involved during the synchronization of movements with sensory information or during the internal generation of movement sequences (2). In a simplified version of these activities, numerous studies have examined how subjects synchronize taps with pacing isochronous auditory stimuli and then continue tapping at the instructed rate without the advantage of the sensory metronome (5). Thus, the cyclic nature of the synchronization-continuation task (SCT) implies that subjects must keep track of the time elapsed since the previous sensorimotor events as well as the time remaining until the next events.

Functional imaging studies have shown that the basal ganglia, the medial premotor cortex (MPC, pre- and supplementary motor areas), the prefrontal and posterior parietal cortex, and the cerebellum are the main nodes of a timing network that is engaged during different time production and perception tasks, including the SCT (6, 7). These studies suggest the existence of a partially overlapping distributed system for the temporal information processing in a variety of sensorimotor contexts that reach a complexity peak during musical cognition and speech, but that also include the production and estimation of single intervals (2, 8).

Neurophysiological studies have shown that cells in MPC are involved not only in controlling self-initiated behaviors, the sequential organization of multiple movements (9), and decision making (10), but also in the production of single intervals in the range of seconds (11). Neuronal activity in MPC is involved in the process of retrieving time instructions from visual cues and shows an increase or decrease in activity associated with the interval duration (11). However, critical and unresolved questions are how MPC is engaged in rhythmic timing behaviors that are driven by sensory or internal events and what neural signals are used to encode the passage of time during a tapping task that has been a backbone in the timing literature. Consequently, in the present study, we examined the response properties of MPC cells during the execution of the SCT in behaving monkeys and found that different types of ramping activity encoded the time elapsed since the previous movement or the time remaining until the next tap in a cyclical fashion.

Results

Selective Activity to the Temporal Context. Two Rhesus monkeys were trained in a version of SCT that included three produced intervals in the synchronization and the continuation phase (Fig. 1*A*, see *Methods*). Auditory interval markers were used during the synchronization condition. Once the animals performed over 75% of correct trials (Fig. S1), we recorded the single cell activity in MPC during task execution (Fig. 1*B*; see *Methods*). The activity of 1,083 MPC cells showed stable responses during SCT. Of these, 703 neurons showed a significant increase in discharge rate during task performance with respect to the key-hold control period and were analyzed further. Interestingly, a large group of these neurons showed a selective increase in discharge rate during the synchronization or the continuation phase ($n = 386$, Fig. 2; ANOVA for task phase, $P < 0.05$). Considering the involvement of MPC in the organization of sequential motor behavior (9), an important question is whether the selective activity during one of the SCT phases was related to the ordinal instead of the temporal aspects of the task. Hence, we also recorded these cells during a sequential reaction time task (SRTT, Fig. 1*C*) that included both similar stimuli and a sequence of tap responses, but where the interstimulus intervals within each trial were random (600-1,400 ms), precluding anticipation and explicit temporal processing (12). Less than 30% of these cells (96 of 386, Fig. S2) maintained their selectivity during the initial or final periods of SRTT. These results suggest that most SCT selective responses were associated with the temporal information processing during the sensory-guided (synchronization) or the internally driven (continuation) cyclic movement production (Fig. 2), and only a fraction of these responses was related to the well known ordinal sequential movement activity in MPC (9).

Single Neuron Activity Before Movement Onset. A large population of neurons showed ramping activity before or after the button press in SCT. Due to the cyclic nature of SCT, it was of the upmost importance to identify with reliability the onset and

Author contributions: H.M. designed research; H.M., W.Z., O.P., L.P., and R.B. performed research; H.M., W.Z., O.P., L.P., and R.B. analyzed data; and H.M., W.Z., and R.B. wrote the paper.

The authors declare no conflict of interest.

This article is a PNAS Direct Submission.

[1]H.M. and W.Z. contributed equally to this work.

[2]To whom correspondence should be addressed. E-mail: hugomerchant@unam.mx.

This article contains supporting information online at www.pnas.org/lookup/suppl/doi:10.1073/pnas.1112933108/-/DCSupplemental.

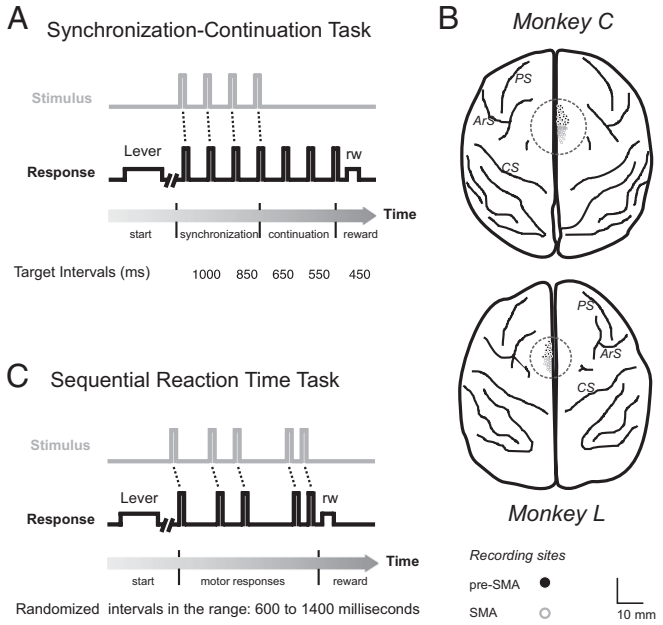

Fig. 1. Behavioral tasks and neuronal recording sites. (*A*) Schematic of epochs in the synchronization-continuation task (SCT), periodic stimuli (gray line), and push button responses (black line). Each trial began when the monkey held a lever. (*B*) MRI surface reconstruction of macaque brain and recording sites in the two monkeys. PS, principal sulcus; ArS, arcuate sulcus; CS, central sulcus; surface bounded by a circle, recording area and medial premotor cortex. (*C*) Schematic of epochs in the sequential reaction time task (SRTT). SMA, supplementary motor area.

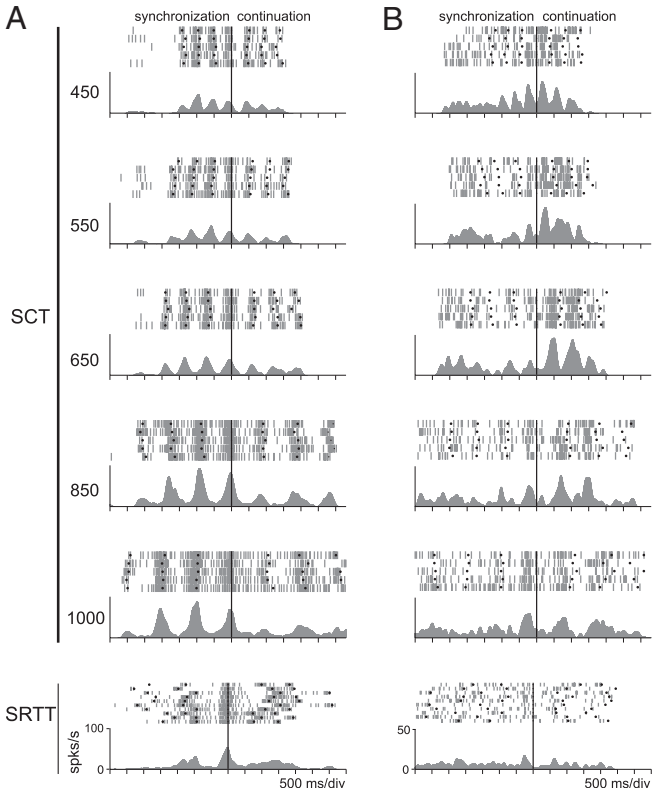

Fig. 2. Ramping activity profiles of two representative cells aligned (thick black vertical line) to the first tap of the continuation period in SCT and to the third tap in SRTT. Every tick mark corresponds to a single spike time stamp in a correct trial; spike density function (SDF) averages are below each raster. The dots represent the button press. (*A*) Synchronization-selective neuron. (*B*) Neuron with differential activity in the continuation phase. Note that the cells do not show ordinal sequence-selective responses during the SRTT in the bottom.

duration of the ramping activity (Fig. 2). Thus, an iterative algorithm was developed to find the best linear regression model that explained the increase or decrease of instantaneous activity with respect to a sensory or motor event using the spike density function (SDF; Fig. S3). With this method, we defined for each produced interval the following ramp parameters: duration, slope, starting and peak magnitude, and the time τ from the peak to the button press. The results of this analysis showed five groups of neurons, three groups whose ramping activity increased overtime reaching a maximum before the button press, and two groups with responses after the button press. Here we describe the former three cell types. One group of cells showed ramps with a similar duration across target intervals (ANOVA, $P > 0.05$; 236 neurons) and were classified as motor ramps (Fig. 3*A*). A second population of ramping cells showed a significant increase in ramp duration as a function of target interval (ANOVA, $P < 0.05$; 163 neurons). A large group of these ramps also showed a significant decrease in slope as a function of target interval (ANOVA, $P < 0.05$; 129 of 163 neurons) and were called relative-timing cells, because in addition to their time modulated climbing activity they all had the tendency to reach their peak magnitude at a similar time before the button press (Fig. 3*B*). Therefore, these cells could signal how much time is left for triggering the button press in the task sequence. An important property of the motor and relative-timing ramps was their sharp decrease in activity after reaching the magnitude peak, suggesting that both cell types were only related to the upcoming movement. In contrast, the third type of ramping activity showed a more complex response. This small group of cells also showed an increase in ramp duration as a function of target interval (ANOVA, $P < 0.05$); however, instead of changing their slope, the cells showed a decrease in ramp starting magnitude as a function of the target interval (ANOVA, $P < 0.05$; 34 neurons; Fig. 3*C*). As with the relative-timing cells, these responses reached their peak magnitude at similar moments before the button press. Nevertheless, in this case, the beginning of the climbing activity was preceded by a monotonic decrease in activity. Thus, the minimum level of activity of the descending responses was systematically lower for longer durations, and this phenomenon was more evident when the activity was aligned to the previous button press (Fig. 3 *C Left*). We called these cells swinging ramps because their responses were characterized by a down-up profile of activation whose fluctuation depth depended on the duration of the target interval.

Population Activity Before Movement Onset. The neural mechanism for the time remaining for a tap during SCT should compute the time of the actual produced intervals during the task execution, instead of the target intervals used to cue the animals. Therefore, we calculated the actual duration of the produced intervals during task performance and regrouped the single trial ramping activity of the 3 cell types according to these durations (from 400 to 950 ms in steps of 50 ms, $n = 12$). We observed that the distribution of produced intervals had a bimodal structure with modes around 450 and 850 ms for the synchronization and continuation phases of SCT. The distribution of produced intervals during SRTT was skewed toward long durations due to the random intervals range of 600–1,400 ms used to avoid prediction (Fig. S4). The neurophysiological data during SCT showed that the duration of the ramping activity increased as a function of produced interval in relative-timing and swinging cells [Kruskal–Wallis test (KW), $P < 0.05$; Fig. S5 and Table S1 for details] and that the ramp slope showed a significant decrease across produced intervals in relative-timing cells (KW, $P < 0.05$). Furthermore, swinging cells showed a significant decrease in the

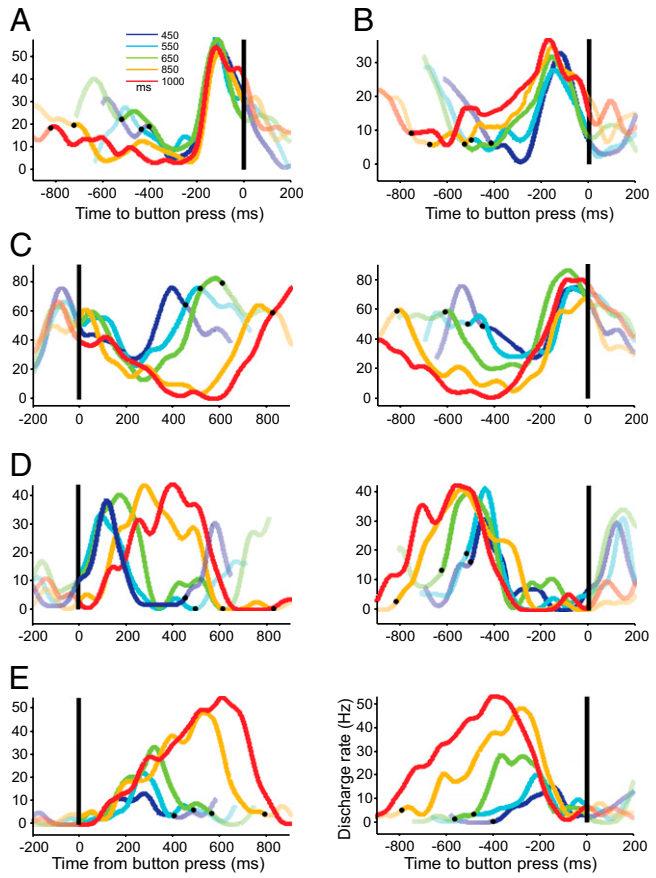

Fig. 3. Average SDF of single cells responding before or after the button press across target intervals in the SCT. (*A*) Neuronal activity of a cell classified as motor because its climbing activity was similar for all target intervals. (*B*) Activity of a relative-timing cell that showed ramps with a significant increase in duration and significant decrease in slope as a function of target interval. (*C*) Neuronal activity of a swinging cell that showed a down-up profile of activation whose fluctuation depth depended on the duration of the target interval. (*D*) Neuronal activity of an absolute-timing cell that shows a increase in its up-down profile of activation as a function of target interval. (*E*) Activity of a time-accumulator cell that showed an increase in discharge rate across target intervals. Cells are aligned to the previous (*Left*) or next (*Right*) button press, with exception of *A* and *B*, were the cells are only aligned to the next button press. The color code for target intervals is described in *A Inset*. The black dots indicate the average time of the previous or next button press. The transparent SDF correspond to the 200-ms period before or after the average produced interval.

ramp starting magnitude as a function of produced interval (KW, $P < 0.05$). The behavior of these variables was different during the SRTT, with practically no modulation across produced intervals for all cell types (Fig. S5; KW, $P > 0.05$). In fact, a significant difference in ramp duration and slope was found between SCT and SRTT for the relative-timing cells (Wilcoxon test, $P < 0.05$, for both variables), whereas for swinging cells a significant difference between the two tasks was observed in ramp duration and starting magnitude (Wilcoxon test $P < 0.05$, for both variables). Hence, the response differences between tasks in the relative-timing and swinging cell populations stress the need for external or internal periodicity to extract temporal contingencies and drive timed responses. In contrast, motor ramps showed a similar duration and slope across produced intervals during SCT and SRTT (Fig. 3*A*), which is a signature for a phasic motor command issued in both behavioral contexts.

We computed the mutual information (MI) between the ramp parameters and the produced intervals (see *SI Text*). The MI is a measure of the statistical dependency between the behavioral variable (i.e., produced interval), and a neurophysiological parameter (i.e., ramp duration). This measure also allows for the identification of the cell activity parameter that best explains a behavioral variable using the same unit of measurement (bits) across the parameters tested (13). The results, shown in Table 1, showed that the MI across the six ramp parameters was smaller for motor cells. In contrast, for relative-timing cells, the MI of the duration of the climbing activity was the largest, followed by the MI of ramp slope. In swinging cells, the ramp starting discharge rate showed a large MI value that was similar to the MI for ramp duration. The MI for the other parameters was small across cell types. Therefore, these results indicate that the change in slope for relative-timing cells and the change in starting ramp magnitude for swinging cells are their distinctive features. Furthermore, these results confirm that ramp duration is a fundamental property for encoding remaining time. It is important to mention that the changes in ramp duration in these two types of cells were not related to the muscular pattern of activation during task performance. The climbing activity of the muscles of the tapping hand/arm was phasic, sharp, and had a peak close to the button press (Fig. S6 and Table S1).

Neural Correlates for Elapsed Time Calculation. Using the algorithm for ramp detection we found another population of neurons that showed an increase followed by a decrease in instantaneous discharge rate when the activity was aligned to the previous button press. The up-down profile of activation can be characterized by the duration of the positive and negative consecutive ramps, the magnitude of the ramps' peak, and the time τ from the button press to the beginning of the positive ramp (Fig. S3). Most of these cells showed a significant increase in the overall duration of the positive and negative consecutive ramps as a function of target interval and were called absolute-timing ramps (ANOVA $P < 0.05$; 304 neurons; Fig. 3*D*). Within this cell population, we found a subgroup of cells that also showed a significant increase in the magnitude of the ramps' peak as a function of target interval, and consequently, were called time-accumulator ramps (ANOVA $P < 0.05$; 124 neurons; Fig. 3*E*). Therefore, these cells could be representing the passage of time since the previous movement, using two different encoding strategies: One functioning as an accumulator of elapsed time where the peak magnitude is directly associated with the time passed, and another where the duration of the activation period is encoding the length of the time passed since the previous movement. Interestingly, when the activity of these two types of responses was aligned to the upcoming movement, it was evident that the end of the downward phase was similar across target intervals (Fig. 3 *D* and *E Right*), suggesting a functional association with the elapsed time encoding cells, as described below.

The duration of the ramps showed a large significant increase across produced intervals in absolute-timing and time-accumulator ramps (KWs, $P < 0.05$; Fig. S7, see Table S2), whereas the peak magnitude showed a larger increase in time-accumulator than in absolute-timing cells across produced intervals (KWs, $P < 0.05$). Conversely, the slope of the initial positive ramp showed a decrease as a function of produced interval that was larger in absolute-timing than time-accumulator ramps (KWs, $P < 0.05$). Furthermore, the MI analysis showed that in both the absolute-timing and time-accumulator ramps the duration of the initial positive ramp was the variable with more bits of information regarding the produced interval, followed by the peak magnitude for the time-accumulator ramps and the slope of positive ramps in the absolute-timing cells (see Table 1).

Multiple Neural Chronometers. The notion of separate groups of cells encoding elapsed or remaining time was supported by the clear bimodal nature of the τ values of the peak in activity; absolute-timing and time-accumulator ramps showed a magnitude peak that was closer to the previous button press (Fig. 4*A*), whereas the τ values for the relative-timing and swinging ramps were closer to the next button press (Fig. 4*B*). The rhythmic

Table 1. Mutual Information in bits for the listed variables across the five types ramping cells

Ramp variable	Motor	Relative-timing	Swinging	Absolute-timing	Time-accumulator
Duration positive	0.253 (7.1)	**0.901 (25.1)**	**0.924 (25.8)**	**0.81 (22.6)**	**0.888 (24.8)**
Duration negative	0.137 (3.8)	0.182 (5.1)	0.417 (11.6)	0.245 (6.8)	0.399 (11.1)
Tau value	0.149 (4.1)	0.161 (4.5)	0.148 (4.1)	0.189 (5.3)	0.215 (6)
Slope positive	0.083 (2.3)	**0.440 (12.3)**	0.268 (7.5)	**0.423 (11.8)**	0.269 (7.5)
Peak magnitude	0.092 (2.6)	0.095 (2.6)	0.333 (9.3)	0.141 (3.9)	**0.69 (19.3)**
Start magnitude	0.078 (2.2)	0.097 (2.7)	**0.955 (26.6)**		

The number in parenthesis correspond to the percent of MI from the maximum, namely, $\log_2(12) = 3.585$ bits. Bold numbers correspond to the larger effects.

structure of SCT may impose the need for both the prediction of when to trigger the next tap and the quantification of the time passed from the previous movement. The noisy character of single temporal ramps, however, implies that the downstream reading neural node cannot rely on single cells to quantify the passage of time or produce accurately timed movements. Therefore, we propose a population code for encoding elapsed or time remaining during SCT, where the reading network adds the magnitudes of a population of individual ramps over time, resulting in a ramp population function $R(t,I) = \frac{\sum_{n=1}^{N} r(t,I)}{N}$, where $r(t, I)$ corresponds to each individual ramp over time (t), from 1 to N total number of ramps of a cell type, and for a particular produced interval (I). Fig. 4*C* shows the ramp population functions for the absolute-timing ramps, where it is evident that the up-down cycle of the $R(t, I)$ increased systematically as a function of the elapsed time since the previous tap. In addition, the $R(t, I)$ for the time-accumulator ramps, depicted in Fig. 4*D*, shows a progressive increase in peak magnitude as a function of the elapsed time since the previous tap. We computed the elapsed time since the previous button-press at different percentages of the peak magnitude of $R(t, I)$, and found that at 90% there was a tight relation between the decoded elapsed time from the ramp population function and the duration of the produced intervals, particularly for absolute-timing cells (Fig. 4*E*). Furthermore, the peak magnitude of the $R(t, I)$ for the time-accumulator showed a clear linear increase as a function of the produced interval (Fig. 4*F*).

Fig. 5*A* illustrates the $R(t, I)$ for the relative-timing ramps; it is clear that these functions showed a sigmoidal behavior and that their duration increased and their slope decreased as a function of produced interval. Therefore, $R(t, I)$ for the time-remaining ramps is a good candidate for the neural computation of time remaining, triggering the tapping movement when it reaches a particular magnitude threshold. These population functions, as well as motor ramps (Fig. 5*B*) and EMGs, showed a slight increase in τ values as a function of produced interval, suggesting a small increase in movement speed for shorter intervals.

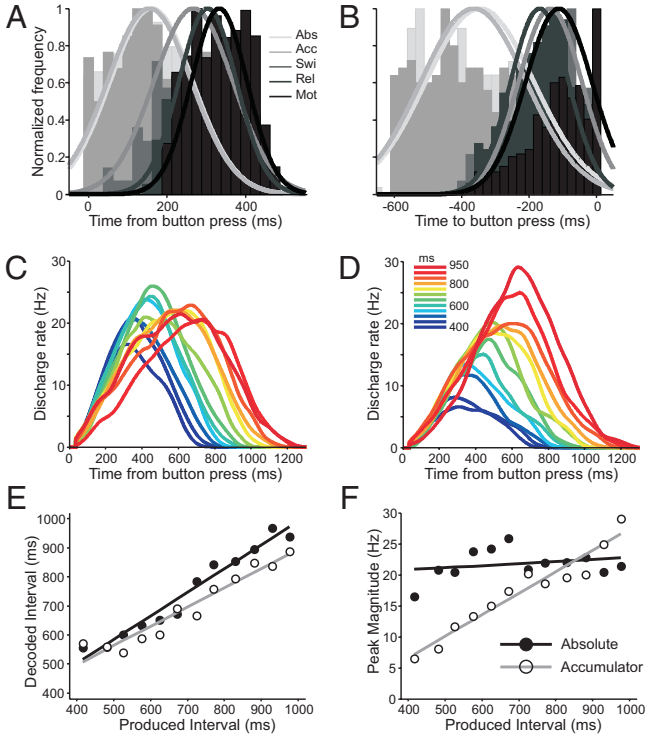

Fig. 4. Histograms of the τ values of the peak of activity with respect to the previous (*A*) or the next (*B*) button press for the five cell types described in the text. Gaussian functions were fitted to the distributions and displayed as lines. Abs, absolute-timing; Acc, time-accumulator; Swi, swinging; Rel, relative-timing; Mot, motor cells. Ramp population functions [$R(t, I)$] for absolute-timing (*C*) and time-accumulator (*D*) cells aligned to the previous button press. The color code corresponds to the duration of produced intervals as depicted in *D Inset*. (*E*) Decoded time as a function of produced interval using 90% of the maximum magnitude of $R(t, I)$ to determine the elapsed time since the button press for absolute-timing (filled circles, black line) and time-accumulator (open circles, gray line) cells. (*F*) Peak magnitude of the $R(t, I)$ as a function of produced interval for absolute-timing and time-accumulator cells. Lines correspond to linear regression fits.

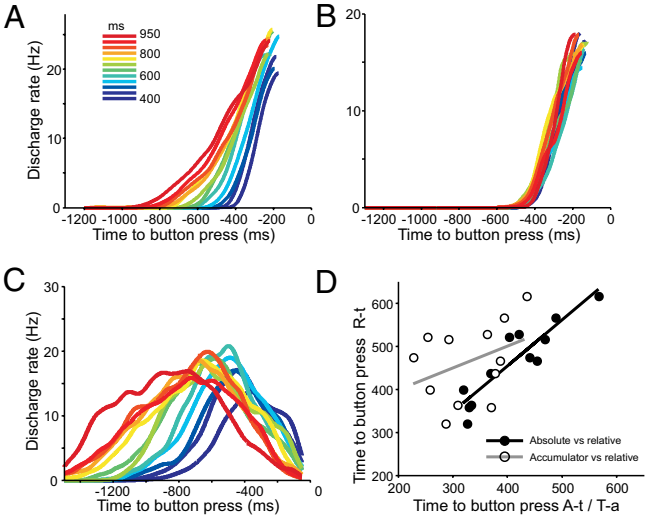

Fig. 5. Ramp population functions for relative-timing (*A*) and motor (*B*) cells aligned to the next button press. (*C*) $R(t, I)$ for absolute-timing cells aligned also to the next button press. The color code corresponds to the duration of produced intervals as depicted in *A Inset*. (*D*) Time to button press of $R(t, I)$ at 14 Hz for absolute-timing (A-t; filled circles, black line) cells or at 12 Hz for time-accumulator (T-a; open circles, gray line) cells plotted against the time to button press associated with the $R(t, I)$ at 7 Hz for relative-timing (R-t) cells.

The multiple neural chronometers should interact at some point in their ramping activity to define the rhythmic structure of SCT. To test this idea, we aligned the $R(t, I)$ of absolute-timing and time-accumulator cells to the upcoming button press (Fig. 5*C*) to compare the functions across cell types for the same behavioral event. Then, we computed the time to button press at different magnitudes of $R(t, I)$ for absolute-timing, time-accumulator, and relative-timing cells with the purpose of finding the discharge rate of the population activity at which these cell types showed a similar temporal profile across produced intervals. Fig. 5*D* shows that the time to button press for the $R(t, I)$ at 14 Hz of absolute-timing cells showed a tight linear relation with the time to button press for the $R(t, I)$ at 7 Hz of relative-timing cells across produced interval durations, suggesting that these cell populations were interlocked at a particular moment in their temporal dynamics. This implies that for all produced intervals there is a magnitude in the $R(t, I)$ where of absolute- and relative-timing cells show a very similar temporal relation with regard to the upcoming button press. In contrast, there was no significant correlation between the times to button press of time-accumulator and relative-timing cells at any magnitude of their $R(t, I)$ (Fig. 5*D*). Therefore, these results suggest that the absolute-timing ramps show some level of interaction with the relative-timing cells during each cycle of time production during SCT. However, it seems that the computation of elapsed time from a tapping movement by time-accumulator cells may not be part of the cyclic organization of timing behavior in SCT.

Discussion

This study investigated the functional properties of MPC neurons during the execution of SCT. Four main findings emerged. First, a large population of cells showed selective responses during the synchronization or continuation phases of SCT, suggesting the existence of partially overlapping neuronal populations engaged in temporal processing during sensory-cued or internally driven tapping behaviors. Second, two different groups of cells may encode the time-remaining for a tapping movement, because they showed ramping activity whose duration increased as a function of produced interval and they had the tendency to reach their peak magnitude at a specific time before the button press. Thus, both cell types could trigger the motor command once they reach a threshold. Interestingly, the relative-timing cells acted as the typical time-to-contact mechanism with a systematic decrease in the ramping slope across interval durations, whereas the swinging cells showed a down-up profile of activation whose fluctuation depth depended on the duration of the target interval. The third main finding was that other two cell populations may represent elapsed time since the previous movement. Both cell types showed a linear increase followed by a linear decrease in activity when aligned to the previous button press. The duration of the up-down cycle of activity in absolute-timing cells was associated with subjective time, whereas, in time-accumulator cells, there was an additional increase in peak magnitude as a function of elapsed time. Finally, the activity of all types of ramping cells was quite variable and, consequently, a population of neurons might be needed for the accurate computation of different aspects of time. Hence, distinct populations of cells in MPC can encode elapsed and remaining times during a multiple interval production task that has a cyclic component and requires the temporal control of behavior cued by auditory stimuli followed by a phase of tapping that is internally timed.

The functional repertoire of MPC cells in the behaving monkey includes the sequential organization of multiple movements, which made us question whether the selective activity during one of SCT phases was related to the ordinal instead of the temporal aspects of the task. However, when we tested the same cells in SRTT, a task that precluded the explicit timing of tappping behavior, we found that less than one-third of the cells maintained their selectivity during the initial or final periods of this control task. Therefore, two fundamental aspects of complex behavior, ordinal sequence and temporal structure, are represented in the activity of MPC cells.

Music inherently consists of auditory processing and motor execution, with a rich temporal and sequential structure. In this respect, SCT is a classical timing task that engages the main-core timing system (2) and has the basic components of music. Hence, the present results suggest that the quantification of elapsed and remaining time during the cyclic sensorimotor loops of SCT might be a basic mechanism for other complex rhythmic behaviors, including music. Nevertheless, some precautions should be followed when extrapolating the neural underpinnings of temporal processing from macaques to humans during SCT, because monkeys cannot synchronize their tapping to the sensory metronome, and their timing variability during the continuation phase is greater than humans' (12).

Cell activity changes associated with temporal information processing have been reported in basal ganglia (14), thalamus (15), area LIP (16, 17), and prefrontal cortex (18, 19), as well as in motor cortex (20) and MPC (11). These areas form different circuits that are linked to sensorimotor processing. Most of these studies have described climbing activity during different timing contexts and time scales. Therefore, the increase or decrease in instantaneous activity as a function of time is a distributed property that includes subcortical areas and the frontal lobe and that may be involved in different aspects of temporal processing. Our results showed that the relative-timing cells showed a monotonic increase in climbing activity that reaches a magnitude threshold to trigger a motor command with a fast decay in activity. This profile of activation is similar to the reported ramps in the locust, pigeons, behaving monkeys, and humans (4) during the computation of time-to-contact in interception and collision avoidance behaviors (21). In contrast, the cyclic decrease–increase of activity observed in swinging cells, where the depth in the decrease phase is related to the duration of the interval produced is, as far as we know, a unique mechanism for the computation of remaining time for an action. The cyclic response of swinging cells may be linking the previous button press with the next one during the execution of rhythmic tapping in SCT. Therefore, the computation of the time remaining for an action by two complementary neural signals may be critical for the execution of SCT.

The calculation of elapsed time from the previous tapping movement might be the counterpart of the relative-timing and swinging cells during the intrinsic sensorimotor loops of SCT. We observed cycles of increase and decrease of activity after tapping movements in absolute-timing and time-accumulator cells that were associated with interval duration when aligned to the previous button press. This finding implies that both the raise and decay in cell activity were encoding elapsed time. In the case of time-accumulator cells, however, the magnitude of the ramping activity might be the critical response variable for encoding the passage of time. Hence, these cells could be the neural correlate of the accumulator element of the scalar timing model used to explain the scalar property of interval timing in a variety of psychophysical measurements (22).

Overall, separate cell populations that either quantify the time passed since a movement or that predict the timing for the next movement are locked at some point in their ramping activity, producing a balanced cyclic mechanism for the execution of movement sequences with a tight temporal structure. This is evident between absolute- and relative-timing cells. Hence, the rhythmic nature of SCT may depend not only on the quantification of different temporal aspects of the task but also on the close interaction between these two cell populations. The present findings suggest that the ability to synchronize with auditory information (which is necessary for playing in a musical ensemble) and the ability to maintain an internal tempo (which is indispensable for any solo performance) might depend on coordinated pattern of activation of cell populations that compute elapsed and remaining time for movement execution.

Methods

General. Two male monkeys (5-7 kg body weight) were trained to tap on a push button in both SCT and SRTT (Fig. 1 *A* and *C*). All of the animal experimental procedures were approved by the Universidad Nacional Autonoma de México Institutional Animal Care and Use Committee and conformed to the principles outlined in the Guide for Care and Use of Laboratory Animals (National Institutes of Health, publication number 85-23, revised 1985).

Synchronization-Continuation Task. The SCT used in this study has been described (12). Briefly, the monkeys were required to push a button each time stimuli with a constant interstimulus interval were presented, which resulted in a stimulus-movement cycle (Fig. 1*A*). After four consecutive synchronized movements, the stimuli were eliminated, and the monkeys continued tapping with the same interval for three additional intervals. Monkeys received a reward if each of the intervals produced had an error < 35% of the target interval. In addition, the monkey could receive a double reward if the intertap interval was <20% of the target interval. Trials were separated by a variable intertrial interval (1.2-4 s). The target intervals, defined by brief auditory (33 ms, 2,000 Hz, 65 dB) stimuli, were 450, 550, 650, 850, and 1,000 ms, and were chosen pseudorandomly within a repetition. Five repetitions were collected for each target interval.

Serial Reaction Time Task. This task was used as a control for neural responses associated with sensorimotor and sequential behaviors. Monkeys were required to push a button each time a stimulus was presented, but in this case the interstimulus interval within a trial was random (600-1,400 ms), precluding the explicit temporalization of tapping (Fig. 1*C*). Monkeys received a reward if the response time to each of the five stimuli was within a 200- to 1,000-ms window. The intertrial interval was as in SCT. Brief auditory (33 ms, 500 Hz, 65 dB) stimuli were used, and 10 repetitions were collected.

Neural Recordings. The extracellular activity of single neurons in MPC was recorded using a system with seven microelectrodes (1-3 MΩ, Uwe Thomas Recording; ref. 23). Structural magnetic resonance imaging was used to localize the recording sites (Fig. 1*B*), where each dot represents a recording site.

Data Analysis. ***General.*** Subroutines written in Matlab (Matworks v. 7.6.0.324) and SPSS (version 12, SPSS, 2003) were used for the statistical analyses. An initial ANOVA was performed for each neuron to identify cells whose activity changed significantly during the recording. Of a total of 1,570 cells recorded in the MPC in both monkeys (1,267 of Monkey 1 and 303 of Monkey 2), 1,083 did not show a statistically significant effect on recording time during the control holding period and were analyzed further.

Ramp detection algorithm. We used an iterative algorithm to detect ramping activity based on the increase or decrease in instantaneous activity for each target duration and for each of the six intervals produced in a sequence during task performance. This algorithm has the following steps (Fig. S2). Step 1: Spike times were convoluted with a Gaussian kernel (σ = 30 ms) to obtain the SDF for each trial. Step 2: SDF was aligned to the stimulus presentation or button press during SCT and SRTT. Step 3: The time of the activity peak was detected. Step 4: The minimum activity time was found, and a regression was performed between SDF and the interval between the minimum and peak times. The activity minimum could be located before or after the peak, defining ramps with positive or negative slopes, respectively. Step 5: Regressions were carried out decreasing, in steps of 20 ms, the interval from the minimum activity to the peak time. Step 6: We considered that the algorithm reached convergence when the regression R^2 decreased by less than 5% on subsequent iterations. Step 7: The best regression model in terms of adjusted R^2 was found. Step 8: A ramp was defined when its peak was above 5 Hz, the duration was larger than 100 ms, and the regression $P < 0.01$. The ramp detection algorithm was performed initially on the average SDF across trials for each stimulus or button press (see Fig. S3 for more details). Only the neurons that showed more than three significant ramps across interval durations were studied further.

Ramp classification. We performed a landmark registration analysis based on a warping algorithm to determine whether the cell activity was better aligned to the stimulus onset or the button press during the synchronization phase of SCT. The results showed that the five types of ramping activity were aligned to the movement rather than the stimulus onset. The iterative algorithm was run on SDF aligned to the first or second button press of a particular interval and ramps were associated to one of these events on the basis of the response consistency for each alignment.

ACKNOWLEDGMENTS. We are grateful to A. P. Georgopoulos as well as to B. Averbeck, M. Chafee, V. De Lafuente, and R. Romo for their fruitful comments on the manuscript. We thank Juan Ortiz and Raul Paulín for their technical assistance. This work was supported by Consejo Nacional de Ciencia y Tecnología Grant 053944, Programa de Apoyo a Proyectos de Investigación e Innovación Tecnológica Grant IN206508, and Fogarty International Research Collaboration Award Grant TW007224-01A1.

1. Diehl RL, Lotto AJ, Holt LL (2004) Speech perception. *Annu Rev Psychol* 55:149–179.
2. Janata P, Grafton ST (2003) Swinging in the brain: Shared neural substrates for behaviors related to sequencing and music. *Nat Neurosci* 6:682–687.
3. Phillips-Silver J, Trainor LJ (2005) Feeling the beat: Movement influences infant rhythm perception. *Science* 308:1430.
4. Merchant H, Georgopoulos AP (2006) Neurophysiology of perceptual and motor aspects of interception. *J Neurophysiol* 95:1–13.
5. Repp BH (2005) Sensorimotor synchronization: A review of the tapping literature. *Psychon Bull Rev* 12:969–992.
6. Coull JT, Vidal F, Nazarian B, Macar F (2004) Functional anatomy of the attentional modulation of time estimation. *Science* 303:1506–1508.
7. Rao SM, et al. (1997) Distributed neural systems underlying the timing of movements. *J Neurosci* 17:5528–5535.
8. Merchant H, Zarco W, Prado L (2008) Do we have a common mechanism for measuring time in the hundreds of millisecond range? Evidence from multiple-interval timing tasks. *J Neurophysiol* 99:939–949.
9. Tanji J (2001) Sequential organization of multiple movements: Involvement of cortical motor areas. *Annu Rev Neurosci* 24:631–651.
10. Hernández A, Zainos A, Romo R (2002) Temporal evolution of a decision-making process in medial premotor cortex. *Neuron* 33:959–972.
11. Mita A, Mushiake H, Shima K, Matsuzaka Y, Tanji J (2009) Interval time coding by neurons in the presupplementary and supplementary motor areas. *Nat Neurosci* 12:502–507.
12. Zarco W, Merchant H, Prado L, Mendez JC (2009) Subsecond timing in primates: Comparison of interval production between human subjects and rhesus monkeys. *J Neurophysiol* 102:3191–3202.
13. Kayser C, Montemurro MA, Logothetis NK, Panzeri S (2009) Spike-phase coding boosts and stabilizes information carried by spatial and temporal spike patterns. *Neuron* 61:597–608.
14. Jin DZ, Fujii N, Graybiel AM (2009) Neural representation of time in cortico-basal ganglia circuits. *Proc Natl Acad Sci USA* 106:19156–19161.
15. Tanaka M (2007) Cognitive signals in the primate motor thalamus predict saccade timing. *J Neurosci* 27:12109–12118.
16. Leon MI, Shadlen MN (2003) Representation of time by neurons in the posterior parietal cortex of the macaque. *Neuron* 38:317–327.
17. Maimon G, Assad JA (2006) A cognitive signal for the proactive timing of action in macaque LIP. *Nat Neurosci* 9:948–955.
18. Brody CD, Hernández A, Zainos A, Romo R (2003) Timing and neural encoding of somatosensory parametric working memory in macaque prefrontal cortex. *Cereb Cortex* 13:1196–1207.
19. Genovesio A, Tsujimoto S, Wise SP (2009) Feature- and order-based timing representations in the frontal cortex. *Neuron* 63:254–266.
20. Lebedev MA, O'Doherty JE, Nicolelis MAL (2008) Decoding of temporal intervals from cortical ensemble activity. *J Neurophysiol* 99:166–186.
21. Lee DN (2009) General Tau Theory: Evolution to date. *Perception* 38:837–850.
22. Gibbon J, Malapani C, Dale CL, Gallistel C (1997) Toward a neurobiology of temporal cognition: Advances and challenges. *Curr Opin Neurobiol* 7:170–184.
23. Merchant H, Battaglia-Mayer A, Georgopoulos AP (2004) Neural responses during interception of real and apparent circularly moving stimuli in motor cortex and area 7a. *Cereb Cortex* 14:314–331.

Supporting Information

Merchant et al. 10.1073/pnas.1112933108

SI Text

Calculation of Mutual Information. Information theory has been an important mathematical tool to study how the spike train of a single neuron or a population of neurons transmits information about a behavioral parameter. The mutual information (MI) is a measure of the statistical dependency between the behavioral variable (i.e., produced interval, $n = 12$) and a neurophysiological parameter (i.e., the single-trial ramp duration, slope, τ value, etc. . . across the cell type population). Thus, the MI between the behavioral variable I and neurophysiological parameter r can be defined as:

$$MI(r,I) = \sum_{r,I} p(r,I) log_2 \left(\frac{p(r,I)}{p(r)p(I)} \right)$$

where $p(r, I)$ is the joint probability of r and I, and essentially tells us how much extra information one gets from the behavioral variable by knowing the outcomes of the neurophysiological parameter (1). The overall probability $p(r)$ of observing the r value of the neurophysiological parameter was obtained by marginalization: $p(r) = \Sigma_I p(r, I)$. The $p(I)$ for produced intervals was calculated from the behavior of the monkeys during the neural recordings (see Fig. S4).

The joint distribution $p(r, I)$ was computed from a count matrix $C(i, j)$, in which each entry (i, j) is the number of times a j value of the ramp single trial parameter was observed for the interval duration i. Hence, the approximation: $p(r,I) = \frac{c(i,j)}{\Sigma_i \Sigma_j c(i,j)}$.

1. Golomb D, Hertz J, Panzeri S, Treves A, Richmond B (1997) How well can we estimate the information carried in neuronal responses from limited samples? *Neural Comput* 9: 649–665.

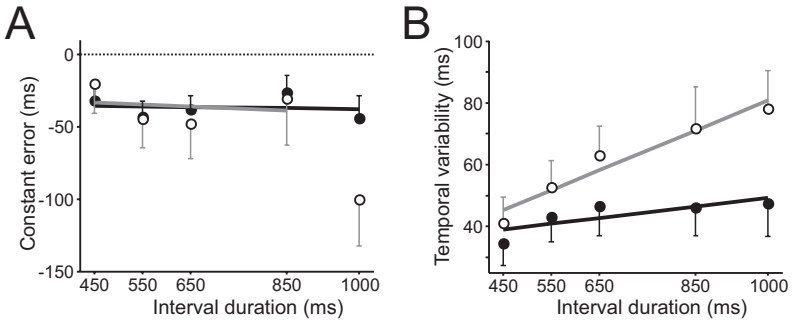

Fig. S1. Timing behavior of the monkeys. (*A*) Constant error (mean ± SEM) as a function of target intervals for the synchronization (filled circles) and continuation (open circles) phases. The linear regression fits between the constant error and interval duration showed slopes close to zero and regression constants around 30 ms, with no significant differences between the synchronization and continuations phase (repeated measures ANOVAs, for slopes: $F(1,772) = 2.84$, $P = 0.092$; for regression constant: $F(1,772) = 2.3$, $P = 0.13$; see *Methods*). Hence, the monkeys were able to produce the target intervals with a small underestimation of around 35 ms across interval durations and task phases. The horizontal line at zero represents perfect accuracy. The straight lines correspond to the best linear fittings, however, for the continuation phase (gray line) the interval of 1000 ms was eliminated of the regression analysis. (*B*) Temporal variability (mean ± SEM) increased as a function of the target intervals for both task phases, following the scalar property of interval timing (Gibbon et al., 1997). The straight lines correspond to the best linear fittings (black: synchronization; gray: continuation).

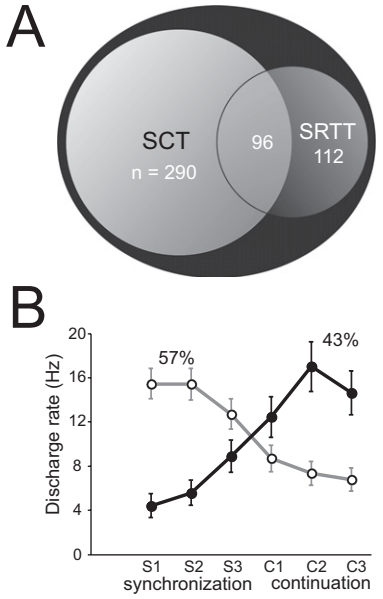

Fig. S2. Analysis of the sequence-related activity during the SCT and SRTT. (*A*) Venn diagrams illustrating the two intersecting sets of phase-related cells during SCT or/and SRTT based on ANOVAs, one for each task, where discharge rate of the neurons was used as dependent variable and the initial and final phase of the tasks were used as factors. The black ellipse denotes the total universe. The areas are proportional to the inset numbers. (*B*) Discharge rate of the phase selective neurons during the sequence of the SCT, with S1–S3 corresponding to the synchronization and C1–C3 to the continuation phase. The mean and SEM of the synchronization-selective responses are depicted as open circles and a gray line, whereas the continuation-selective responses are shown in filled circles and a black line. The percentages indicate the proportion of synchronization- and continuation-selective cells.

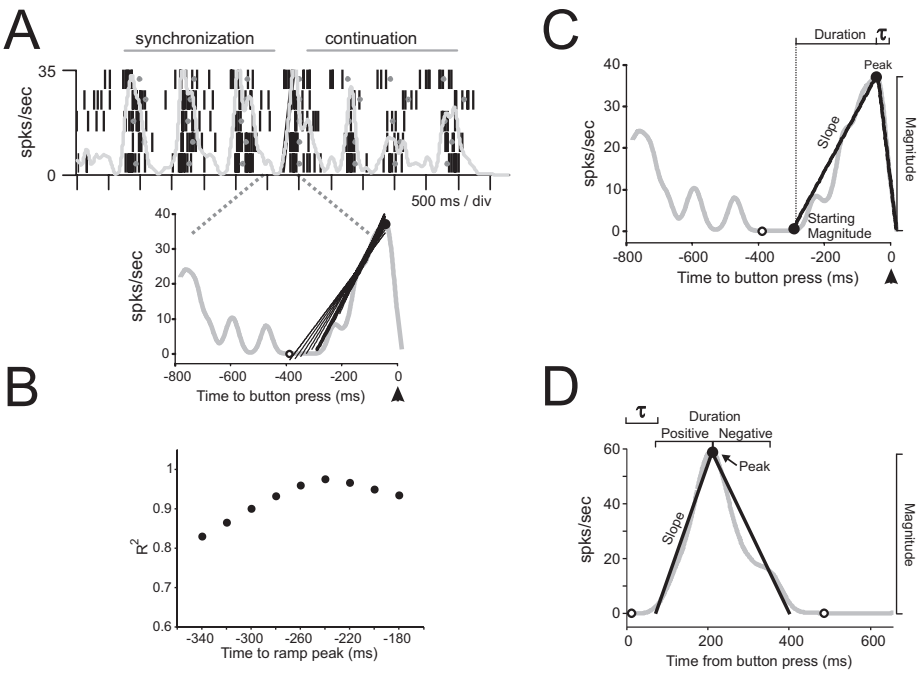

Fig. S3. Iterative algorithm used to find the best regression model to explain the increase or decrease of instantaneous activity over time with respect to a sensory or motor event. (*A Upper*) Raster plot and mean SDF (gray function) of a ramping cell aligned to the first tap of the continuation phase. (*Lower*) The region indicated by the dotted lines in *Upper*, where a series of linear regression functions are displayed, including the best model identified by the algorithm shown as the thicker line. (*B*) Regression R^2 as a function of the time to ramp peak for the example depicted in *A*. (*C*) Parameters that were extracted from the linear regression model for the motor, relative-timing and swinging ramps. (*D*) Parameters that were extracted from the two consecutive linear regression models for the absolute-timing and time-accumulator ramps. Only the neurons that showed more than three significant ramps on the average SDF across interval durations of at least one of the six produced intervals in the SCT sequence, where the significant ramps showed consistent positive or negative slopes, were studied further. Subsequently, the ramp algorithm was performed for each trial on these neurons. This second step was carried out with three purposes: (*i*) To eliminate the cells that showed phasic activity with different response onset latencies across trials, which can produce an artificial activity ramp on the average SDF. (*ii*) To perform the ANOVAs on single trial ramps that allowed the classification of motor, relative-timing, and swinging cells for neurons with consistent responses to the second button press; or the classification of absolute-timing or time-accumulator cells for neurons with consistent responses to the first button press. (*iii*) To carry out the regrouping of single trial ramps as a function of the produced interval and performed the subsequent population analyzes.

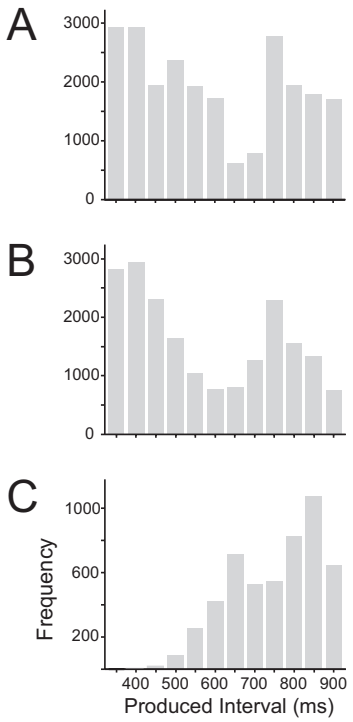

Fig. S4. Distributions of the duration of produced intervals during the synchronization (*A*) and continuation (*B*) phases of SCT, and during the SRTT (*C*) for both monkeys.

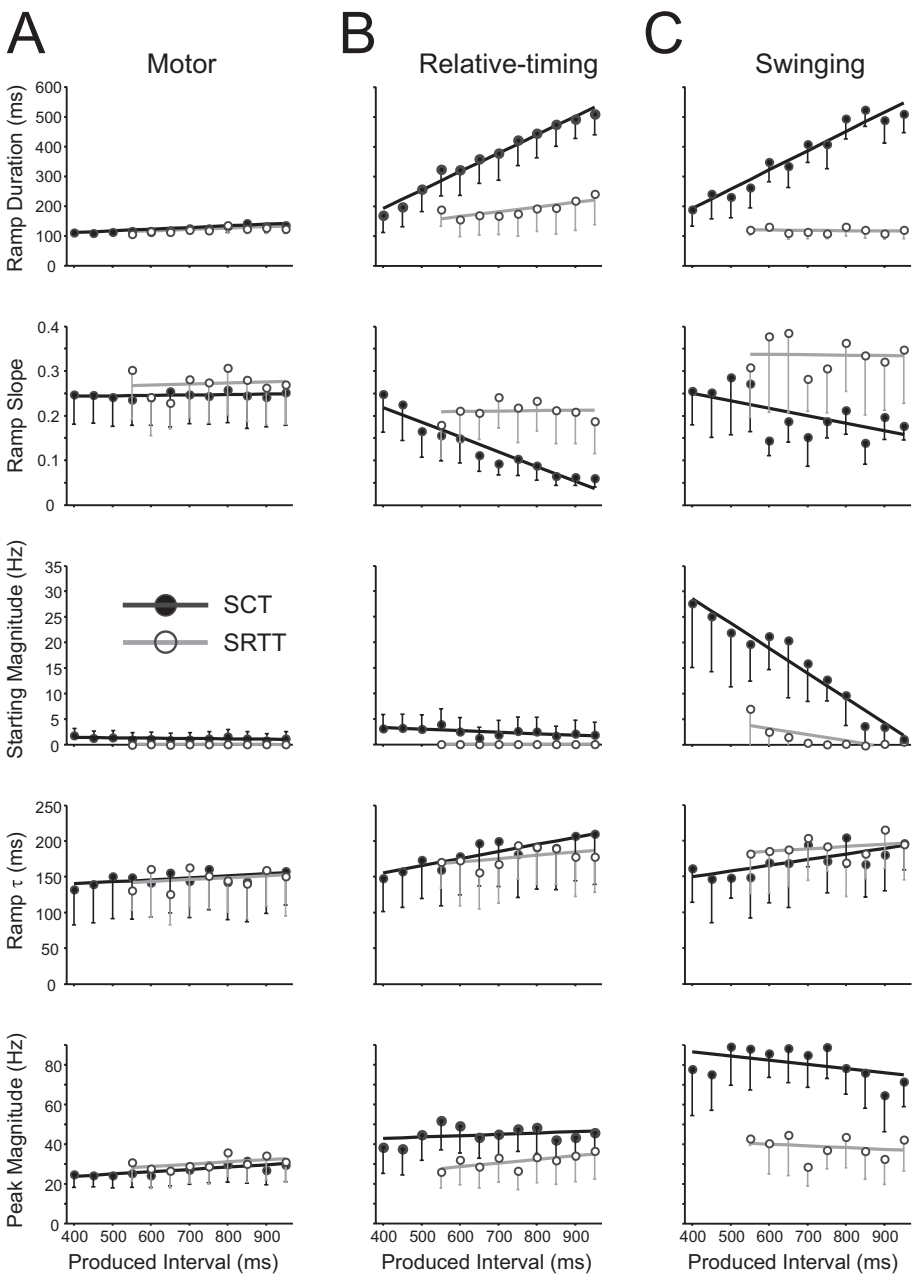

Fig. S5. Mean (± SEM) of the ramp duration, slope, discharge rate at the beginning of the ramp (starting magnitude), τ value, and peak magnitude as a function of the produced interval. (*A*) Motor cells. (*B*) Relative-timing cells. (*C*) Swinging cells. Lines correspond to linear regression fits. SCT: filled circles, black line; SRTT: open circles, gray line.

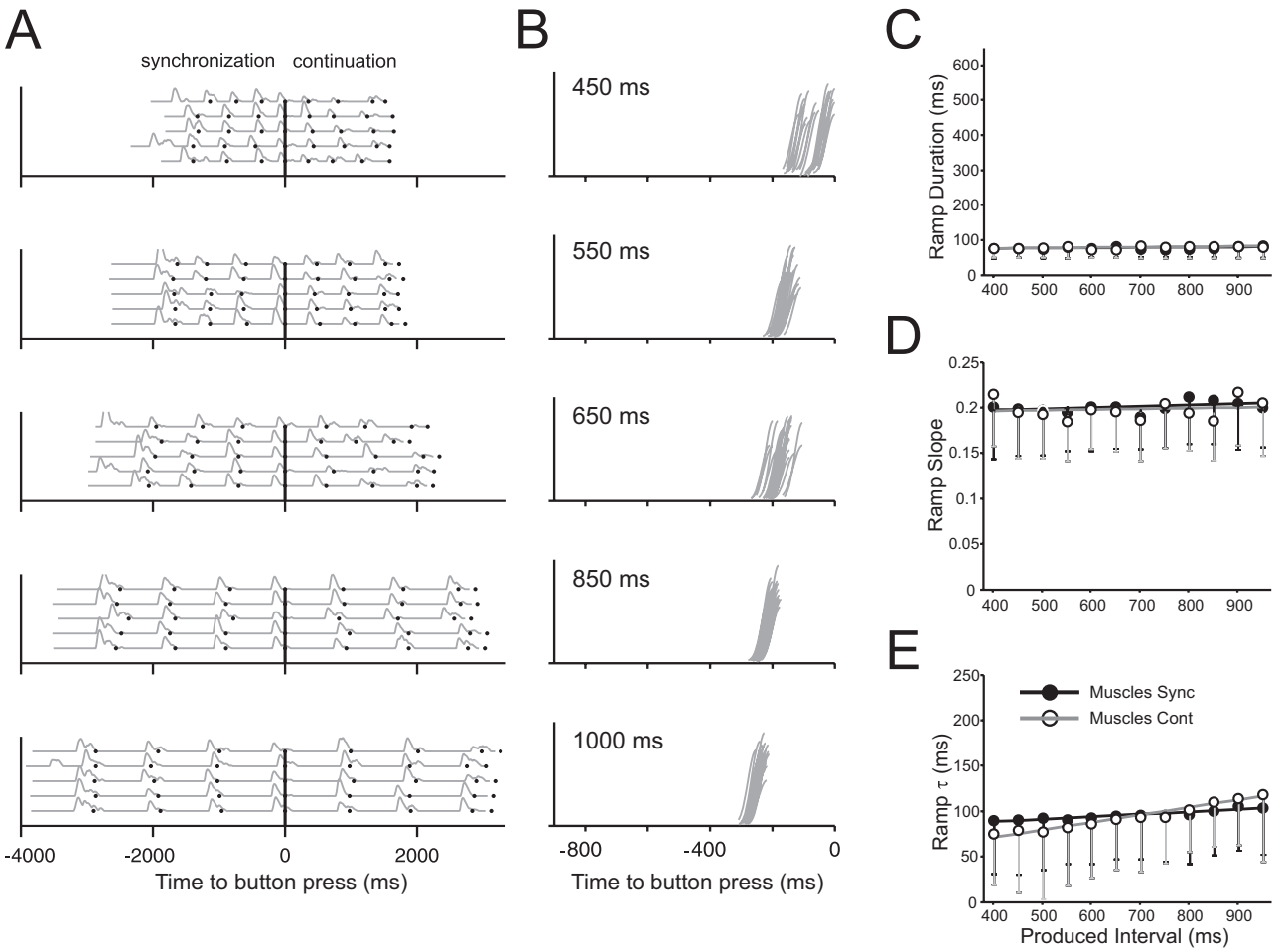

Fig. S6. (*A*) Raster plot for the EMG activity of the *triceps brachii* of monkey 2 during the SCT aligned to the first continuation tap. Same conventions of Fig. 2. (*B*) The corresponding ramps of the *triceps brachii* EMG detected by the iterative algorithm. Ramp duration (*C*), slope (*D*), and τ value (*E*) as a function of the produced interval for the population of EMGs with significant ramping activity. The EMG was recorded in the same two monkeys in separate sessions from the neural recordings using intramuscular, multistranded, teflon-coated wire electrodes. EMG activity was recorded bilaterally in the following muscles for both monkeys: triceps brachii, biceps brachii, deltoideus (anterior, middle, and posterior), extensor digitorum communis, extensor digitorum 2,3, flexor digitorum sublimis, rhomboideus major, trapezius, pectoralis major, and latissimus dorsi.

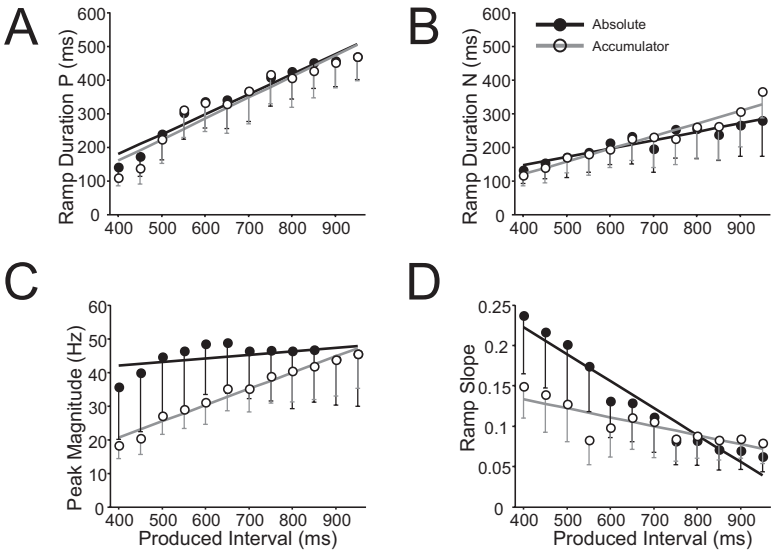

Fig. S7. Mean (± SEM) of the ramp duration for the positive ramp (*A*), the ramp duration for the negative ramp (*B*), the peak magnitude (*C*), and the slope of the positive ramp (*D*) as a function of produced interval, for absolute timing (filled circles, black line) and time-accumulator (open circles, gray line) cells.

Table S1. *P* values and χ^2 for the Kruskal–Wallis tests performed for ramp duration, slope, starting magnitude, peak magnitude, or Tau value as depending variable and using the produced interval as factor

	Duration		Slope		Starting magnitude		Peak magnitude		Tau value	
Cell	*P*	χ^2	*P*	χ^2	*P*	χ^2	*P*	χ^2	*P*	χ^2
Relative-timing	0	1138.8	0	847	0.06	19	0	147.5	0	82.5
Swinging	0	150.3	0	38.1	0	76.9	0	32.6	0.02	22.5
Motor	0.09	16.1	0.105	17.1	0.79	7.07	0	44.8	0.001	24.9
Muscles synch.	0	39.8	0.23	13.9					0.004	33.9
Muscles cont.	0	69.9	0.006	32.8					0	226.6

Kruskal–Wallis tests are less sensitive to unequal sample sizes. Starting magnitude is defined as the discharge rate of the cells at the beginning of the climbing activity. These values are shown for the relative-timing, swinging and motor ramps, as well as for the muscular activity during the synchronization and continuation phases separately.

Table S2. *P* values and χ^2 for the Kruskal–Wallis tests performed for Ramp duration, slope, peak magnitude, or Tau value as depending variable and using the produced interval as factor

	Absolute-timing		Time-accumulator	
Ramp variable	*P*	χ^2	*P*	χ^2
Duration positive	0	1530.6	0	966.4
Duration negative	0	447.3	0	486.9
Tau value	0	158.1	0	175.4
Slope positive	0	1041	0	558.9
Peak magnitude	0	176.8	0	771.2